

Fluorescence Imaging Study of Film Coating Structure and Composition Effects on DNA Hybridization

Bingquan Yang, Klavdiya Gordiyenko, Andreas Schäfer, Seyed Mohammad Mahdi Dadfar, Wenwu Yang, Kristina Riehemann, Ravi Kumar,* Christof M. Niemeyer, and Michael Hirtz*


Hybridization of surface-bound DNA with complementary strands is the basis of many biotechnological applications. Herein, the structure of interfacial coatings between substrate and bound DNA is a crucial element for hybridization behavior. Herein, three reactive surfaces for constructing DNA-sensing platforms, namely, plain gold films on silicon, poly(bisphenolA-co-epichlorohydrin) (PBAG) surfaces with a brush-like bilayer structure, and dibenzocyclooctyne monolayers (both on glass), are compared. Fluorescence imaging is employed to survey the effect of coating structure and conformation on hybridization performance. To better understand the interfacial structural properties and chemistry of the coated films, atomic force microscopy, water contact angle measurements, and X-ray photoelectron spectroscopy are employed to characterize the surface morphology. DNA probe microarrays are created on the different platforms via microchannel cantilever spotting, and their performance for hybridizing with the DNA counterparts is assessed. While all three platforms work reliable for DNA detection, a protein-binding assay reveals that PBAG surfaces offer the highest hybridization efficiency among these approaches. The results of the present work have significant implications for comprehension of the interactions between the DNA hybridization efficiency and the physico-chemical properties of surface coatings and can inform the fabrication of DNA sensors.

1. Introduction

Biosensing is a significant field in biological research,^[1–4] and the DNA-based biosensors are highly regarded.^[5,6] The development of DNA biosensors has gained substantial attention over the last decades because it has tremendous potential in the application of disease diagnosis and forensics,^[3,7] in particular also for diagnostic of viral diseases.^[8,9] Many ways of DNA detection and also the use of DNA-based sensors for detection of DNA and other targets are emerging.^[10,11] Still, basic nucleic acid-sensing strategies are often based on the hybridization of nucleic acids, such as single-stranded DNA (ssDNA) probes that specifically bind their complementary target strand.^[12,13] First, ssDNA probes with a complementary sequence to the target are immobilized on the sensor interface or surface, then, the targeted complementary ssDNA can hybridize with the probe and bind the target for detection.^[12] Different technologies have been developed for tethering DNA probes to substrates.^[14,15]

Among them, the patterning into microarrays has become one of the most popular and efficient fabrication approaches for sensing platforms since it evolved in the 1990s,^[16] thus broadly used in

B. Yang, S. M. M. Dadfar,^[†] W. Yang, R. Kumar, M. Hirtz
Institute of Nanotechnology (INT) and Karlsruhe Nano Micro Facility (KNMF)
Karlsruhe Institute of Technology (KIT)
Hermann-von-Helmholtz-Platz 1, 76344 Eggenstein-Leopoldshafen,
Germany
E-mail: ravi.kumar@kit.edu; michael.hirtz@kit.edu

 The ORCID identification number(s) for the author(s) of this article can be found under <https://doi.org/10.1002/anbr.202200133>.

^[†]Present address: I. Physikalisches Institut (IA), AG Biophysik, RWTH Aachen University, 52074 Aachen, Germany

© 2023 The Authors. Advanced NanoBiomed Research published by Wiley-VCH GmbH. This is an open access article under the terms of the Creative Commons Attribution License, which permits use, distribution and reproduction in any medium, provided the original work is properly cited.

DOI: 10.1002/anbr.202200133

K. Gordiyenko, C. M. Niemeyer
Institute of Biological Interfaces (IBG-1)
Karlsruhe Institute of Technology (KIT)
Hermann-von-Helmholtz-Platz 1, 76344 Eggenstein-Leopoldshafen,
Germany

A. Schäfer
nanoAnalytics GmbH
Heisenbergstraße 11, 48149 Münster, Germany

K. Riehemann
Physical Institute and Center for Nanotechnology (CeNTech)
University of Münster
Wilhelm-Klemm-Straße 10, 48149 Münster, Germany

DNA hybridization,^[17] protein detection,^[18] and other biosensing systems.^[19–22] Normally, spot uniformity, density of immobilized DNA probes, and repeatability are known as primary factors for detecting probe microarray sensitivity and reliability, and these factors are strongly influenced by the physical and chemical properties of the sensor platform interface.^[23–25] Furthermore, steric hindrance between the DNA probe and the interface, as well as steric hindrance between adjacent probes and electrostatic forces, all affect the hybridization efficiency and capacity in surface hybridization.^[26] As a result, researchers have focused their attention on the morphology properties and structural architectures of the platforms in order to better understand the effects of interactions between the immobilized DNA probe assembly and the surface conformations on hybridization behavior.

To achieve robust microarrays, a stable binding of the DNA probe to the substrate is key.^[13] Here, in particular, thiolates have been used as a reactive bridge for covalent binding of DNA oligomers to gold films because of its ease of use, chemical availability, and ability to produce thin and uniform films. A covalent Au-S bond forms by spontaneous reactions of thiolated oligonucleotides and gold surfaces thus immobilizing the DNA probe on the surface.^[27,28] Studies have shown that the gold-sulfur bond is less stable than bonds between sulfur and silver or copper, and this limits development and large-scale manufacturing to some extent.^[29] However, silver and copper are seldom used for in vivo analysis due to their strong toxicity to living systems and their ability to easily oxidize, which readily attracts carbon-based contaminants from the ambient environment leading to difficulties in forming densely packed molecular layers.^[13] Therefore, gold-based system became a more desirable candidate for attaching thiol-conjugated derivatives as a result of its good biocompatibility and favorable qualities in optics and electronics.^[29] Gold-based systems are in particular suited for measuring and monitoring DNA hybridization via surface plasma resonance.^[30] Microarrays on the other hand are mostly read-out via fluorescence imaging.^[31,32] Here, gold-based platforms are unfavorable, as they can quench fluorescence when fluorophores get near to the surface.^[33] However, there are also alternatives to gold-based interfaces, also able to accommodate thiolated DNA probes. Click reactions have become a popular procedure for conjugation of biomolecules because of its high yields, mild reaction conditions, and compatibility with a wide range of reactive moieties. Different functional interfaces allowing specific click chemistry reactions, e.g., alkyne-based,^[34,35] alkene-based,^[36,37] and epoxy-based surfaces are available.^[17,38]

Additionally, the hybridization behavior of the surface-immobilized ssDNA probes highly depends on the probe packing density, probe conformation, and the interface structure and configuration.^[39,40] Several studies have proposed numerous schemes for immobilizing DNA probes in upright conformations on the interfaces, i.e., gold film-coated surfaces,^[41,42] biotinylated coatings,^[43,44] polymer-modified interfaces,^[45,46] and adsorption of DNA probes via a thiol incorporated at one end.^[26] Brush-like interfaces or brush-like probes can also strengthen hybridization efficiency because of the lower steric hindrance as compared to the directly adsorbed probes on metal interfaces (Au, Ag, or Cu).^[26] To the best of our knowledge, no direct comparison on the differences in DNA hybridization behavior on various platforms with different surface topographies and

compositions, such as self-assembled monolayers (SAMs), metal-based films, and polymer-based coatings, have been undertaken yet.

Therefore, in this work, three different platforms [dibenzocyclooctyne (DBCO)- and PBAG-modified surfaces and plain gold surfaces] were compared to study the influence of surface chemistry, topography, and conformation on DNA hybridization. The DBCO-modified surface is a SAM surface with cyclooctyne species that through thiol/yne reaction can click to thiolated molecules. The PBAG-modified surface is a grafted bilayer polymer system with epoxide terminals that can bind to SH-DNA via thiol/epoxide reaction. The gold-coated surface is prepared by physical vapor deposition and can react to thiolated-oligomers via Au-S bonds. To evaluate the hybridization behavior and efficiency on these platforms, ssDNA probe (22 or 44mer) microarrays were patterned by microchannel cantilever spotting (μCS), followed by hybridization with a complementary oligonucleotide conjugated either with a fluorescent dye or a biotin moiety. Finally, DNA-directed immobilization (DDI) was implemented for additional binding tests. DDI is a mild and powerful technique to create functional protein patterns on surfaces by aid of surface-bound oligonucleotides, as capture probes, and protein-DNA conjugates bearing the complementary ssDNA.^[47] The DDI method is chemically mild and highly efficient to produce (micro)patterned patterns of proteins on surfaces and, due to its robustness, has found multiple applications ranging from biosensing and biomedical diagnostics to fundamental studies in biology and medicine at the single cell level.^[48,49] Utilizing DDI, protein-binding tests were performed to quantitatively determine the hybridization efficiency on different platforms by measuring fluorescence intensity (**Figure 1**).

2. Results and Discussions

2.1. Characterization of the Sensing Platforms

Prior to spotting of the DNA probe microarrays on the different platforms, the surface wettability, morphology, architecture, and composition were investigated by static water contact angle (WCA), atomic force microscope (AFM), ellipsometry, and X-ray photoelectron spectroscopy (XPS) to characterize the basic surface parameters and morphology (**Table 1**).

In general, WCA testing is a facile method to identify whether the expected molecules are modified on the substrate or not^[50,51] because different molecules lead to different surface tension and show different WCA value.^[52] Thus, static WCA measurements were performed on hydroxylated, DBCO-terminated, and PBAG-modified surfaces for up to three-month post modification (**Figure 2a**, S1, Supporting Information). Initially, the plasma-activated, thus hydroxylated glass sample shows a near zero WCA. However, over the time of storage (see methods), the WCA of the hydroxylated sample increases and approaches the bare glass value (approx. 46°) again after 28 days. The DBCO-terminated glasses exhibit less hydrophilicity, with an initial WCA at around 18°, stabilizing at approximately 63° after 4 weeks. The change of WCA on DBCO-modified and hydroxylated surfaces can likely be ascribed to the gradual decay of residual hydroxyl groups after the initial functionalization.^[34] The WCA of freshly prepared amino-terminated surfaces (as basis

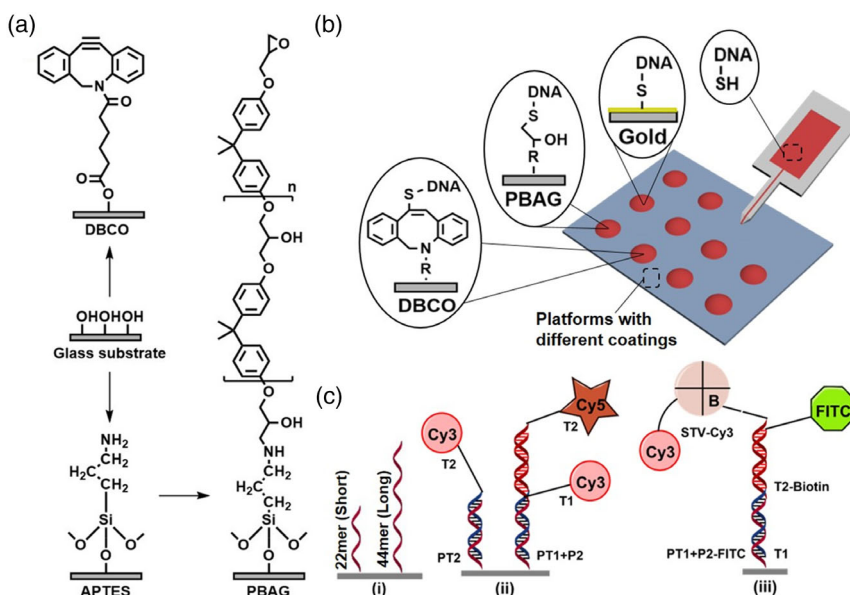


Figure 1. a) Schematic diagram of the modification processes of DBCO- and PBAG-modified platforms (PBAG polymer average weight $40.000 \text{ g mol}^{-1}$; average weight of the monomeric subunit is 348 g mol^{-1}). b) Thiolated DNA probe microarrays patterned by μCS on modified platforms, c) hybridization and protein binding on DNA arrays.

Table 1. Static WCA, roughness, and ellipsometric thickness values of different platforms (mean \pm s. \pm S. D.).

Items	WCA [°]	Roughness (R_a , nm)	Thickness [nm] ^{a)}
Glass	46.0 ± 1.5	0.135 ± 0.086	–
Aminated	44.0 ± 0.9	0.205 ± 0.099	1.4 ± 0.1
Gold-film	53.0 ± 1.4	0.519 ± 0.172	$100^b)$
DBCO-modified	63.0 ± 1.3	0.212 ± 0.107	1.5 ± 0.2
PBAG-modified ^{c)}	33.0 ± 1.3	0.386 ± 0.143	27.6 ± 2.7

^{a)}Ellipsometric thickness was measured on silicon samples prepared in parallel with glass samples. ^{b)}Nominal thickness as of the evaporation process. ^{c)}PBAG polymer average weight $40.000 \text{ g mol}^{-1}$; average weight of the monomeric subunit is 348 g mol^{-1} .

step for PBAG modification) shows a value at around 31° , raising to 44° after about 4 weeks (curve not shown). After “grafting to” the PBAG layer onto the NH_2 -silanized surfaces, the WCA maintains at around 33° over the monitored period. This indicates a good stability of the film and the brush structures overlaying the whole surface (thus residual groups on the surface are covered from the start).

In addition to the WCA, surface roughness (root-mean-square roughness (R_a)) was evaluated via AFM and film thicknesses measured via ellipsometry for the different modifications (Figure 2, Table 1). The bare glass possesses a very smooth interface with a roughness of $(0.135 \pm 0.086) \text{ nm}$. After coating with different materials the roughness rises. As shown in Figure 2c and S2, Supporting Information, the DBCO-terminated and NH_2 -terminated surfaces

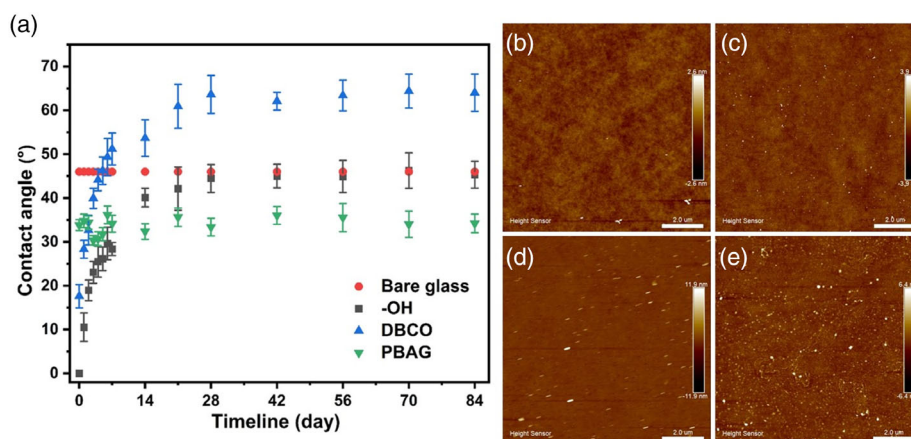


Figure 2. a) Recording of static WCA on bare glass, hydroxyl (-OH), DBCO, and PBAG platforms for up to three months after the modification. AFM images of b) bear glass, c) DBCO-terminated, d) PBAG-terminated, e) gold coated. All scale bars are equal to $2 \mu\text{m}$.

exhibit roughnesses of (0.212 ± 0.107) nm and (0.205 ± 0.099) nm, respectively. This is consistent with the roughness of SAMs,^[50] implying that the DBCO and amino group layers are successfully immobilized on the surface. The ellipsometric thickness of DBCO-treated and NH_2 -treated samples are (1.5 ± 0.2) nm and (1.4 ± 0.1) nm, respectively, again consistent with a successful SAM formation.^[53] After “grafting to” the PBAG layer onto the NH_2 -treated surfaces, the roughness increased further to (0.386 ± 0.143) nm and the ellipsometric thickness reached (27.6 ± 2.7) nm. The gold-coated surface (prepared with 100 nm thickness of Au layer) displays a slightly higher value of roughness of (0.519 ± 0.172) nm compared with the other surfaces.

To confirm also the chemical modifications, XPS was performed on the samples (Figure 3). As can be seen in Figure 3a,b, the nitrogen composition of the bare glass is about 0.7 at%, while after functionalization with -NH_2 and DBCO species, the nitrogen compositions increase to 3.0 and 0.9 at%, respectively, confirming that the amino and DBCO compounds attached to the surface.^[34] However, the nitrogen composition declined to 1.4 at%, when the second layer (PBAG) was grafted to the aminated surface. This can be understood, as there are no nitrogen atoms existing in the scaffold of the grafted PBAG, thus changing the elemental composition

of the surface. The high-resolution XP spectra in the N 1s region (Figure 3b) of -NH_2 , PBAG-, and DBCO-functionalized surfaces all show two distinct peaks. The first one, located at 400.0 eV, is attributed to the amino and the amide groups the second (402.2 eV) can be attributed to the secondary amine groups.^[54] Furthermore, the XP spectra of the C 1s region (Figure 3c) show that only the spectrum of the PBAG-modified sample shows an additional peak at 287.0 eV, which probably stems from the epoxy groups on the PBAG backbone.^[55] As further indication of PBAG attachment, the ratio of $(\text{C-C, C-H}):(\text{C-O})$ is raised from 2.76 to 3.51 after grafting of the PBAG layer. For the gold surface, the core-level spectra of the Au 4f region show two strong peaks observed at 84.0 and 87.7 eV, respectively, which can be attributed to the metallic Au.^[56] All in all, the XP spectra confirm that the expected compounds are presented on the surfaces and surface modification was successfully implemented.

2.2. DNA Hybridization on Different Platforms

In order to generate microarrays for DNA hybridization, thiol-conjugated DNA probe sequences were spotted on the different

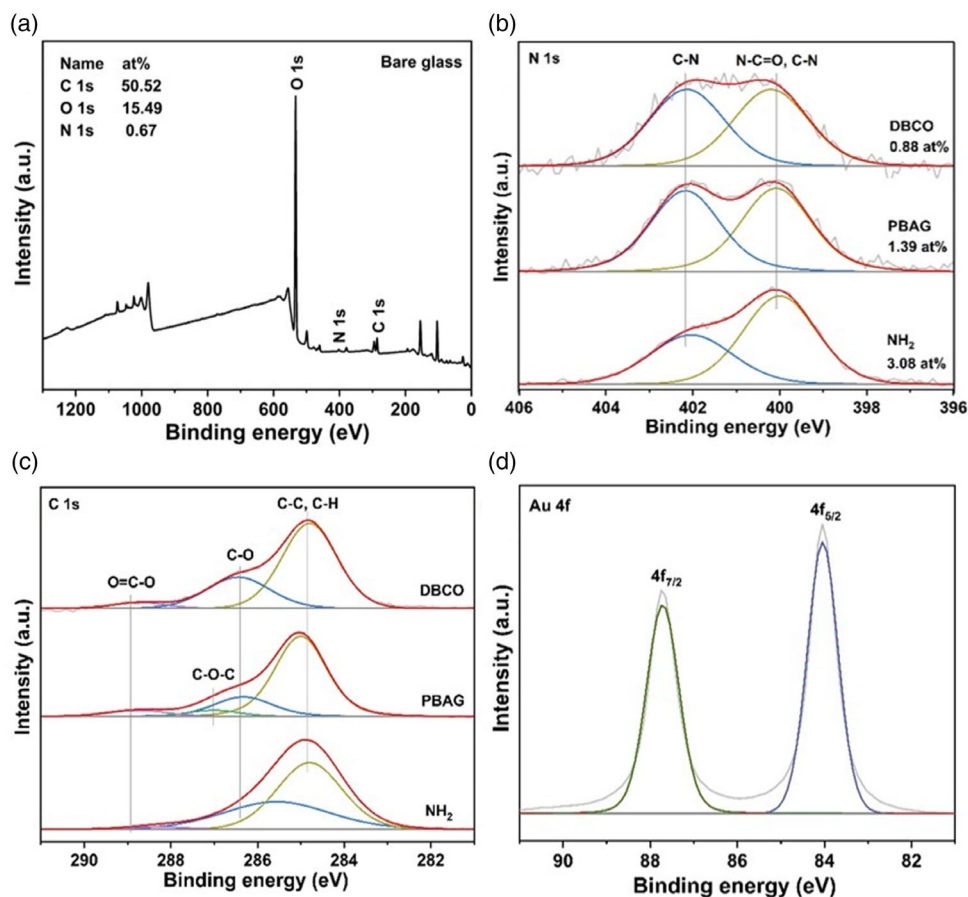


Figure 3. XP spectra of different chips. a) XP wide spectrum of bare glass surface, b) high-resolution XP spectra at N 1s region of aminated (bottom), PBAG-terminated (middle), and DBCO-terminated (top) chips, c) high-resolution XP spectra at C 1s region of aminated (bottom), PBAG-terminated (middle), and DBCO-terminated (top) chips, d) high-resolution XP spectra at Au 4f region of gold-coated surface. The gray curves are the measured intensity, while the colored curves are the best fit of the measured intensity by the single components contributing (blue, green, and purple) and the resulting sum of contributions (red).

platforms via μ CS. To ensure complete reactions (thiol/epoxy, thiol/alkyne, and thiol/gold) and to obtain saturated density of the immobilized probes, the spotted samples were allowed to rest at room temperature overnight before washing off the excess ink solution. Prior to hybridization, samples were blocked by bovine serum albumin (BSA) to prevent unspecific adhesion of DNA to the surfaces. Probes of two different lengths were employed, 22mer sequences (“short”) and 44mer sequences (“long”). The DDI protein-binding tests were conducted on oligomer arrays containing long probe segments (44mer), which were hybridized with two short target sequences (both 22mer). After hybridization, samples were assessed by fluorescence microscopy.

As a first test of successful probe immobilization and hybridization on the different platforms, short probe segments (PT2, 22mer) were spotted into microarrays, followed by hybridized with fluorescently labeled ssDNA targets (T2-Cy3, 22mer), and the results are summarized in **Figure 4**. Obviously, hybridization occurred on all platforms as evident by the microarray becoming visible in fluorescence. On the PBAG-coated sample (Figure 4a), the microarray spot features stand clearly out over the background after hybridization. On the DBCO-terminated surface (Figure 4b), the hybridized pattern is also visible, though signal intensity is weaker. An interesting phenomenon was found on the gold-coated samples, as after hybridization, the arrays were barely seen in fluorescence when imaged in air (Figure 4c). Only in solution patterns were clearly visible (Figure 4d). This can be

understood considering that the fluorophores in the DNA targets are being quenched by the gold surface in air conditions, due to the DNA sequences lying down to the surface bringing the fluorophore even nearer to the gold film. This increases the energy or electron transfer between the fluorophore and the surface, thus leads to nonradiative relaxation of the excited state.^[33] Under liquid, the DNA sequences are in a more upright conformation, and the enlarged distance between the gold interface and the fluorophore weakens the quenching effect by the gold, making the patterns observable in fluorescence. On these ground, the fluorophore-surface interactions on the gold-coated chips cause challenges for surface fluorescence analysis.^[26] In addition, the effects of the pH value of the phosphate-buffered saline (PBS) solution used as liquid on the fluorescent signal of the Cy3-conjugated target probes on the gold surface were also studied, but no significant impact was found (Figure S3, Supporting Information). Consequently, and to stay near physiological pH, the nearly neutral PBS buffer was used for all further experiments. Figure 4f shows the summary of the relative fluorescence intensity of the hybridized samples on PBAG-coated (12317.43 ± 1079.56 a.u.), DBCO-coated (6926.22 ± 1406.44 a.u.) and gold-coated (2900.93 ± 243.69 a.u.) surfaces. Clearly, the PBAG surface exhibits the highest fluorescence intensity of the three platforms, followed by DBCO and gold. Additionally, the PBAG sample shows less background comparing to the DBCO sample, which is favorable to the fluorescent signal readout. The difference in the platforms’ performance will be caused by

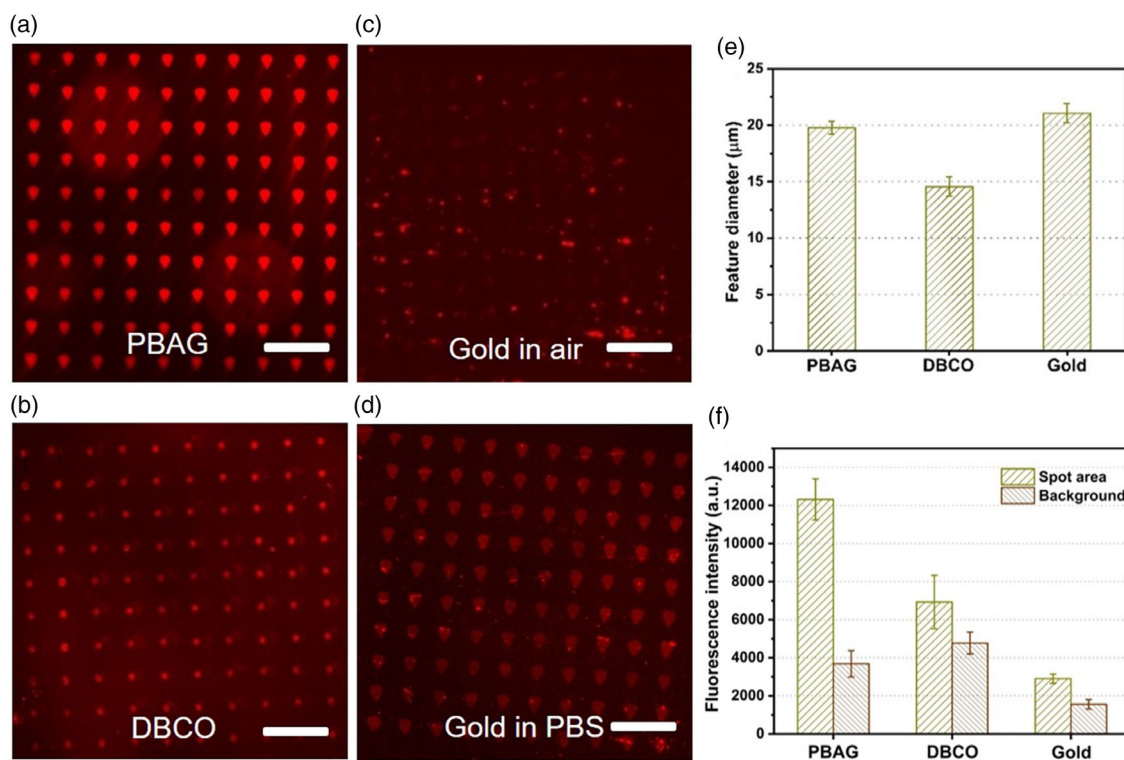


Figure 4. Hybridization of the target T2-Cy3 (red) with the probe PT2 dot arrays on different platforms, a) on PBAG surface, b) on DBCO surface, c) on gold surface (image captured in air, showing almost complete quenching of the fluorophore), and d) on gold surface (image captured in PBS solution, showing a more clear signal of the target bound to the probe array). e) Histogram of feature size (denoted by spot diameter) in DNA detection array on samples in image (a), (b), and (d). f) Summary of the relative fluorescence intensity (hybridized spots and background) collected on images (a), (b), and (d), respectively. The exposure times of the images are 1 s, and scale bars are equal to 100 μ m.

a combination of several effects. 1) The efficiency of probe binding and resulting probe density in the microarray spots, 2) influence of the surface itself in hybridization with the target DNA, e.g., over surface charge effects, and 3) interference with the fluorescent readout by quenching of the fluorophore. Here, increasing roughness of a surface can raise the number of possible binding sites resulting in a higher probe density. While the gold surface is the roughest of the tested platforms, it suffers from the fluorophore quenching, thus lowering overall performance. The surfaces' influence on the hybridization itself is harder to assess. In order to exclude a direct influence of the (underlying) glass surface itself on probe immobilization and hybridization, a control experiment with probe PT1-FITC (22mer, green fluorescent) was done on bare glass. After washing, no fluorescence was observed (Figure S4, Supporting Information), thus the glass itself does not significantly bind DNA on itself.

As the fluorescent signal on the gold-coated sample is by far the weakest one among the three hybridization strategies, probably due to the quenching effect of gold, limiting the application prospect in fluorescence read-out microarrays. It was not further considered in the next experiments.

Next, two-step hybridizations were performed, in order to demonstrate a more complex DNA assembly. For this, two different short targets (both 22mer) were used to hybridize with a probe bearing a complementary long segment (44mer) on PBAG- and DBCO-modified surfaces one after another (Figure 5). For PBAG surfaces, microarrays of probes bearing long sequence (PT1 + P2, 44mer) were spotted via μ CS and then hybridized subsequently with the short targets T1-Cy3 (first, 22mer) and T2-Cy5 (second, 22mer). On first incubation, the microarray appears in Cy3-channel of the fluorescence (Figure 5b), and after second incubation, also in the Cy5-channel. In a similar protocol but with differently labeled targets, a long sequence probe (PT1 + P2-FITC, 44mer) was spotted into a microarray and then subsequently hybridized first with a nonfluorescent short target (T1, 22mer) and then with a fluorescently labeled second short target (T2-Cy3, 22mer). First, the microarray is stably visible in the FITC-channel fluorescence (Figure 5e), via the probe-conjugated fluorophore. On the second incubation, the microarray becomes visible also in the Cy3-channel (Figure 5f) proving the assembly of the second target. It should be noted that Cy3/Cy5 and FITC/Cy3 can potentially build FRET pairs.^[57] However, in the current configuration, on DBCO samples, no transfer from FITC to Cy3 is expected, as the Cy3-channel filter excitation is at longer wavelength as needed to excite FITC. For the PBAG surface, Cy3 is obviously not quenched, thus if at all only partial transfer can occur, which would decrease Cy3 signal on PBAG. Therefore, the quantized fluorescence intensity collected on PBAG- (Figure 5b) and DBCO-modified (Figure 5f) surfaces again confirms that the PBAG surface exhibits advantages in DNA hybridization by showing a higher signal intensity and less background fluorescence.

In the last set of experiments, the PBAG and DBCO platforms were assessed for DDI-like protein immobilization. For this, both surfaces were prepared with microarrays spotted from the same fluorescently labeled probe with long sequence (PT1 + P2-FITC, 44mer) and then hybridization with the short targets (T1 and T2-Biotin). In a final incubation step, the microarrays were incubated with a fluorescently labeled protein (streptavidin-Cy3) that

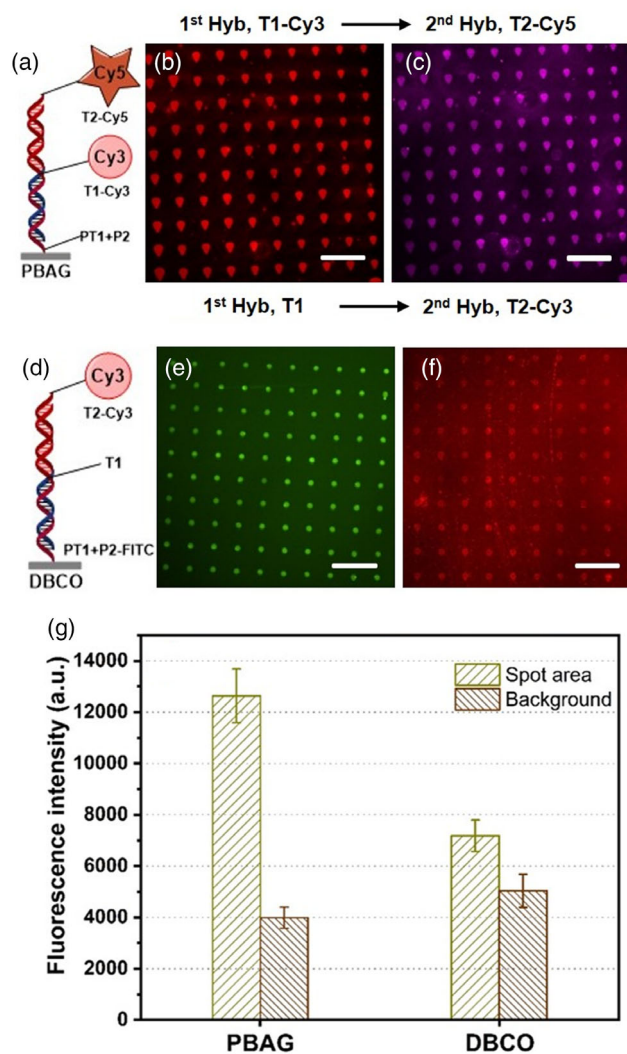


Figure 5. Hybridization (Hyb) of two ssDNA targets one after another with a long probe sequence. a) Schematic drawing of hybridization configuration for (b) and (c). The ssDNA targets b) T1-Cy3 (red) and c) T2-Cy5 (magenta) were incubated on PBAG-modified substrate after immobilization of PT1 + P2 on the surface. d) Schematic drawing of hybridization configuration for (e) and (f). Hybridization of e) T1 and f) T2-Cy3 (red) with the PT1 + P2-FITC (green) probe array on DBCO-modified surface. g) Summary of the relative fluorescence intensity (spot area and background) collected on images (b) and (f). The exposure times are 1 s, and scale bars are 100 μ m.

can then self-assemble over the biotin-avidin interaction.^[19,58] Figure 6 shows the results of the protein binding assay on the DNA patterns. After patterning, on both platforms, the probe microarray is clearly visible in FITC-channel (Figure 6a,b). After hybridization and protein incubation, the microarrays are also visible in the Cy3-channel indicating successful immobilization of the protein (Figure 6c,d). The fluorescence intensity of the coupled streptavidin on the hybridized DNA arrays is (9673.33 ± 879.38) a.u. on the PBAG surface and (5621.22 ± 606.44) a.u. on the DBCO surface, respectively. On the whole, the DNA hybridization efficiency on PBAG-modified chips is around 40% higher than it on DBCO-modified chips according to the fluorescence intensity. A possible

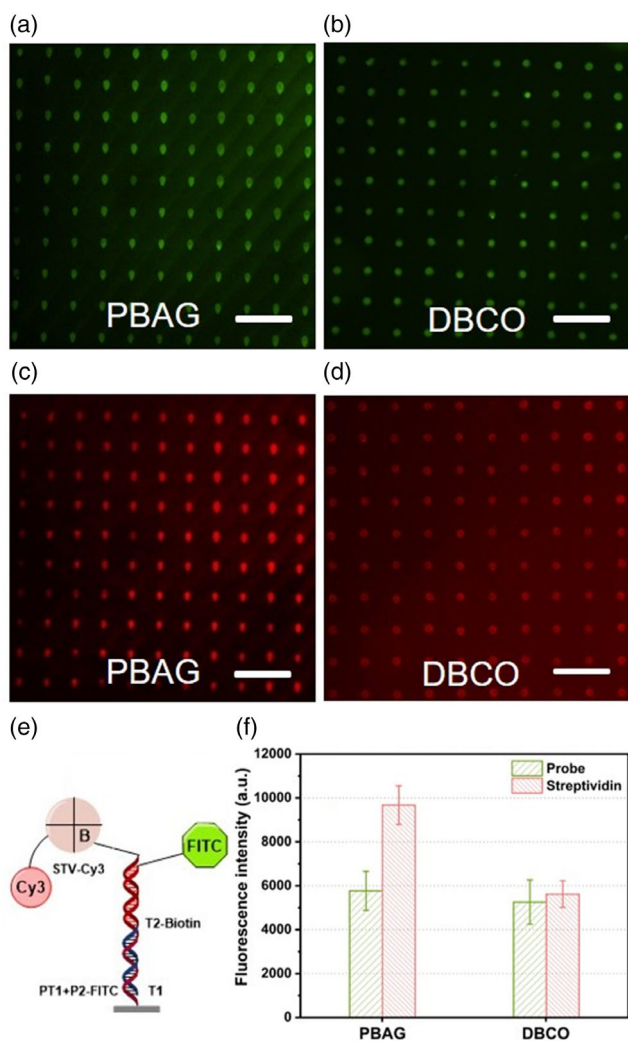


Figure 6. Fluorescence images captured on PT1 + P2-FITC (green) immobilized arrays on a) PBAG-treated and b) DBCO-terminated chips after hybridization with T1 and T2-Biotin. Incubation of SA-Cy3 (red) on c) PBAG substrate, and on d) DBCO substrate after hybridization with T1 and T2-Biotin. e) Schematic drawing of DNA hybridization and protein-binding configurations. f) The relative fluorescence intensity probe (green) and streptavidin (red) collected on picture (a), (b), (c), and (d), respectively. The exposure times are 1 s, and scale bars are 100 μm .

reason could be that the “grafting to” bilayer polymer, PBAG-treated surface, declines the activated sites for DNA probe immobilization and lowers the steric hindrance, hence leading to a higher hybridization efficiency.

3. Conclusion

In this research, an investigation of the effects of three different kinds of platforms (gold on silicon, epoxide-functionalized polymer on glass, and alkyne-terminated SAM on glass) on DNA hybridization behaviors and efficiency via fluorescence imaging was performed. It was found that—while in principle all three platforms are smooth enough for the immobilization of

ssDNA probe arrays via μCS —the gold-coated surface was the roughest one, and the DBCO-SAM surface showed the lowest roughness. The hybridization experiments on gold-based samples showed that the strand orientation had a distinct influence on detection sensitivity, as it induced quenching of fluorophores when the probes lay flat on the surface. While in principle, all platforms could be used for μCS -based construction of probe arrays, the omitting of quenching effects makes DBCO- and PBAG-surfaces much more considerable for construction of high signal-to-noise probe arrays. PBAG consistently offered a lower background fluorescence in comparison to DBCO-surfaces, indicating less unspecific binding of targets. Overall, PBAG-modified platforms that had a bilayer polymer brush structure demonstrated the highest efficiency of hybridization evaluated by fluorescent imaging, almost 40% higher than on DBCO-treated samples. The results inform the fabrication of DNA sensors on polymer-based interfaces to gain a higher hybridization efficiency in fluorescent imaging detection strategies.

4. Experimental Section

Materials: Glass coverslips (18 \times 18 mm) were obtained from VWR (Germany). Methanol was purchased from Merck (Germany). Acetone, chloroform, acetic acid, glycerol, toluene, dichloromethane, hydrogen peroxide (H_2O_2), ammonium hydroxide solution (28–30%, NH_3), (3-aminopropyl)triethoxysilane (APTES) and poly(bisphenol A-co-epichlorohydrin), and glycidyl end-capped (PBAG, polymer average weight 40.000 g mol^{-1} ; average weight of the monomeric subunit 348 g mol^{-1}) were purchased from Sigma-Aldrich (Germany). Dibenzylcyclooctyne-NHS ester (DBCO-NHS) was obtained from Jena Bioscience (Germany). Ethanol absolute was bought from VWR (Germany). Bovine serum albumin (BSA), phosphate-buffered saline (PBS), dibasic potassium phosphate (K_2HPO_4), potassium phosphate monobasic (KH_2PO_4), and trehalose dihydrate were bought from Sigma-Aldrich (Germany). Tween 20 was obtained from Euroimmun (Germany). Ultrapure water (18.2 $\Omega\text{m cm}$) was produced in lab by an Arim Pro system from Sartorius (Germany). All the chemicals were used as received and without any purification processing.

All single-stranded oligonucleotides containing thiol-conjugated probes (PT1-FITC, PT2, PT2-FITC, PT1 + P2, PT1 + P2-FITC) and target oligomers (T1, T1-Cy3, T2-Cy3, T2-Biotin) were purchased from Sigma-Aldrich (Germany), and the sequences are shown in **Table 2**.

Substrates Modification: The detailed preparation protocol for PBAG slides can be found elsewhere.^[59] Briefly, the glass coverslips or silicon slides were cleaned with an aqueous solution consisting of 14.3% NH_3 and 14.3% H_2O_2 in ultrapure water at 150 $^\circ\text{C}$ for 20 min. Immediately after, the slides were washed with ultrapure water, ethanol and ultrapure water again, and dried under a nitrogen stream. Afterward, the slides were immersed in a freshly prepared 1% APTES solution (95% methanol, 5% H_2O , 1 mM acetic acid) for 20 min to obtain amino silane-derived layers on the slides. The substrates were then washed with ethanol, ultrapure water, and acetone and dried under a N_2 stream. Finally, the slides were soaked in an acetone solution containing 5% PBAG over night at room temperature. When finished, the slides were washed with acetone, dried under nitrogen stream, and stored at -20°C .

To prepare DBCO-terminated glass surfaces, coverslips were cleaned by chloroform, ethanol, and water using an ultrasonic bath for 5 min each to remove the surface organic contaminants and then dried with a stream of nitrogen. Followed by, the glass slides were hydroxylated by oxygen plasma (10 sccm O_2 , 0.2 mbar, 100 W) in an ATTO system, Diener electronics (Germany) for 2 min. Without delay, the glass slides were functionalized with DBCO by immersing in a DBCO-NHS ester solution (1 mg mL^{-1}) in dichloromethane overnight at room temperature. Finally, the glass slides were rinsed thoroughly with dichloromethane,

Table 2. Sequence of oligonucleotides.

Oligonucleotide	Sequence (5'-3')
PT1-FITC (22mer)	[6FAM]-GGA CGA ATA CAA AGG CTA CAC G-[ThiC3]
PT2	GTG GAA AGT GGC AAT CGT GAA G-[ThiC3]
PT2-FITC	[6FAM]-GTG GAA AGT GGC AAT CGT GAA G-[ThiC3]
PT1 + P2 (44mer)	CGA CGA ATA CAA AGG CTA CAC GGTG GAA AGT GGC AAT CGT GAA G-[ThiC3]
PT1 + P2-FITC	[6FAM]-GGA CGA ATA CAA AGG CTA CAC GGTG GAA AGT GGC AAT CGT GAA G-[ThiC3]
T1	C GTG TAG CCT TTG TAT TCG TCC
T1-Cy3	[Cyanine3]-C GTG TAG CCT TTG TAT TCG TCC
T2-Cy3	[Cyanine3]-C ACC TTT CAC CGT TAG CAC TTC
T2-Cy5	[Cyanine5]-C ACC TTT CAC CGT TAG CAC TTC
T2-Biotin	[Biotin]-C ACC TTT CAC CGT TAG CAC TTC

acetone, ethanol, and water and then dried by blowing with N₂. The completed chips were stored in dark in a desiccator.

The gold-coated Si substrates were prepared by evaporating 100 nm Au on 7 nm Cr. Prior to use, the gold substrates were sonicated by chloroform, ethanol and water 5 min each, and then dried with a stream of nitrogen. After that further cleaning with an oxygen plasma cleaner for 2 min (10 sccm O₂, 0.2 mbar, 100 W).

Ink Preparation: The ink solutions were prepared by dissolving oligonucleotides in a mixture of Trehalose buffer and glycerol (v/v, 8:2) at a concentration of 100 μM. The added glycerol was to avoid premature drying of the ink and also acted as an ink carrier. The Trehalose buffer containing 200 mM K₂HPO₄, 200 mM KH₂PO₄, 0.5% v/v trehalose-dihydrate, and 0.1% v/v Tween 20. The ink solutions were stored in 4 °C in dark until further usage.

Printing Methodology: The printing process was conducted on an NLP 2000 platform (NanoInk, USA), which equipped with an SPT probe acting as a patterning tool (SPT-S-C30S or SPT-S-C10S, Bioforce Nanosciences).^[60] Before starting lithography, for loading the ink properly and promoting ink flow, the probe was cleaned by oxygen plasma (10 sccm O₂, 0.2 mbar, 100 W, 2 min). Immediately after, the probe was loaded with 0.25 μL of ink solution. To obtain ordered pattern and control ink flow, the relative humidity of the printing chamber was governed at range of 30–40%. In addition, dot patterns were designed of 10 × 10 spot arrays with a pitch of 50 μm in each direction, and a dwell time of 0.5 s was used for all patterns.

Hybridization for Detection Procedures: Arrays containing probe oligonucleotides spotted by SPL tips were allowed to at rest overnight to complete the binding between the thiol groups contained in oligonucleotides and the DBCO or PBAG or gold surfaces and then washed three time by pipetting with PBS to remove the excess ink solution. Straight after, the sample was blocked with 50 μL BSA for 30 min to diminish nonspecific binding of the target DNA or the protein. Subsequently, 50 μL of target ssDNA (1 μM) was covered on the sample surface at room temperature for 1.5 h to perform hybridization process, then washed with PBS three times, and then dried with nitrogen. For the second hybridization, the similar procedure aforementioned was used.

Protein Binding on Hybridized Biotinylated DNA Array: To characterize the feasibility of protein binding on hybridized chips, a mixture containing streptavidin-Cy3 (1 mg mL⁻¹) and PBS (v/v, 1:100) was given on the previously hybridized with the biotinylated oligonucleotide arrays at room temperature for 30 min. As the sample surface has already been blocked by BSA in the hybridization step and the protein incubation followed immediately after hybridization, no additional BSA blocking step was applied. The existing BSA film still acted as efficient antifouling protection against unspecific protein adhesion. Afterward, the chips were washed by pipetting on and off PBS three times and then dried by blowing with nitrogen.

Characterization: The wettability of different surfaces was characterized with an OCA-20 contact angle analyzer (Data Physics Instruments GmbH, Germany) per measuring of static contact angle. In general, the data

recording was conducted by performing a 3 μL water droplet on the surface, and the measurement was repeated three times for each sample to get the mean standard deviation. The same samples were remeasured for obtaining the WCA over time, while avoiding previously measured areas on the respective sample. In between measurements, the samples were stored in a desiccator cabinet (dark environment, room temperature of ≈21 °C, and relative humidity ≈35% r.H). The morphology micrographs of substrates were acquired on a Bruker atomic force microscopy (AFM, Dimension Icon, Bruker, Germany). Analyses were determined at tapping mode in air with aluminum-coated silicon tip (40 N m⁻¹, 325 kHz, HQ: NSC15/Al BS, MicroMasch, Germany) and with rotated tip shape. Each sample was scanned in 10 × 10 μm scale and repeated on three different sites. The thickness of the self-assembled DBCO and NH₂ monolayers and the brush-like PBAG layer was measured by spectroscopic ellipsometry (M 2000, Woollam Co., Inc., Lincoln NE, USA) on silicon substrates in dry conditions at an incident angle of 65° in the wavelength range of λ = 370–900 nm. Every sample was measured three times. All measurements were evaluated with an optical box model on the software CompleteEase, and silicon substrates were all fitted with standard values for Si and SiO₂ as defined in the software. The thickness and the optical properties of the molecular layers were fitted with a Cauchy relation model. A Nikon Eclipse 80i upright fluorescence microscope (Nikon, Japan) was hired in this work to capture the fluorescent pictures, the microscope was equipped with a CoolSNAP HQ2 camera (Photometrics, USA), an Intensilight illumination (Nikon, Japan), and Texas Red and FITC and Cy5 filters set (Nikon Y-2 E C⁻¹). Samples on DBCO- and PBAG-treated substrates were observed in dry conditions, but for samples on gold substrates were performed in PBS solution unless noted for samples in dry conditions.

Apart from this, the analysis of chemical compositions of the surface in each step was identified by X-ray photoelectron spectroscopy (XPS) using a Thermo Scientific K-Alpha system (XPS, Thermo Fisher Scientific, East Grinstead, UK) with a base pressure of about 2 × 10⁻⁹ mbar. Excitation was done using monochromatic Al-Kα-X-rays. The energy calibration of the system was done according to ISO 15472:2001 using copper, silver, and gold reference samples. The transmission function was determined using the build in thermo standard method on a silver reference sample. Quantification of the measurement results was done using modified scofield sensitivity factors. A 400 μm X-ray spot was used for the analysis. On nonconducting samples, a flood gun was used for compensating charging.

Statistical Analysis: All data shown in this work were described as means ± standard deviations. The values of fluorescence intensity were obtained by an on-board software (NIS Elements AR 5.02.01, Nikon) of the microscope. Here, the 100 features for each array were selected via the detect particle function and the mean intensity for each feature was recorded. These intensities were then used to calculate the mean and standard deviation for a given array. The original data of WCA, thickness, and roughness were obtained by measuring 3 random points of each sample, and the means and standard deviations were computed in Excel (Microsoft) by STDEVA formula.

Supporting Information

Supporting Information is available from the Wiley Online Library or from the author.

Acknowledgements

This work was carried out with the support of the Karlsruhe Nano Micro Facility (KNMFi, www.knmf.kit.edu), a Helmholtz Research Infrastructure at Karlsruhe Institute of Technology (KIT, www.kit.edu). B.Y. acknowledges support by the China Scholarship Council fellowship (CSC, www.csc.edu.cn).

Open Access funding enabled and organized by Projekt DEAL.

Conflict of Interest

The authors declare no conflict of interest.

Data Availability Statement

The data that support the findings of this study are available from the corresponding author upon reasonable request.

Keywords

DNA hybridization, DNA microarrays, fluorescent imaging, functional surfaces, microchannel cantilever spotting

Received: August 29, 2022

Revised: November 28, 2022

Published online:

- [1] H. J. Park, J. H. Yoon, K. G. Lee, B. G. Choi, *Nano Convergence* **2019**, *6*, 9.
- [2] H. R. Culver, M. E. Wechsler, N. A. Peppas, *ACS Nano* **2018**, *12*, 9342.
- [3] J. Wu, Y. Qu, Q. Yu, H. Chen, *Mater. Chem. Front.* **2018**, *2*, 2175.
- [4] Y. Zhang, J. Sun, L. Liu, H. Qiao, *J. Diabetes Complications* **2021**, *35*, 107929.
- [5] J. Liu, L. Yan, S. He, J. Hu, *Nano Res.* **2022**, *15*, 3504.
- [6] V. C. Diculescu, A.-M. Chiorcea-Paquim, A. M. Oliveira-Brett, *TrAC Trends Anal. Chem.* **2016**, *79*, 23.
- [7] A. I. Lopez-Lorente, *Anal. Chim. Acta* **2021**, *1168*, 338474.
- [8] X. Tao, X. Chang, X. Wan, Y. Guo, Y. Zhang, Z. Liao, Y. Song, E. Song, *Anal. Chem.* **2020**, *92*, 14990.
- [9] Q. Wang, J. Wang, Y. Huang, Y. Du, Y. Zhang, Y. Cui, D. M. Kong, *Biosens. Bioelectron.* **2021**, *197*, 113739.
- [10] N. Bellasai, R. D'Agata, G. Spoto, *Anal. Bioanal. Chem.* **2021**, *413*, 6063.
- [11] Y. Hua, J. Ma, D. Li, R. Wang, *Biosensors* **2022**, *12*, 183.
- [12] A. Kasry, A. Nicol, W. Knoll, *Appl. Phys. B* **2021**, *127*, 68.
- [13] I.-W. P. Chen, C.-C. Chen, S.-Y. Lin, C.-H. Chen, *J. Phys. Chem. B* **2004**, *108*, 17497.
- [14] S. Reisewitz, H. Schroeder, N. Tort, K. A. Edwards, A. J. Baumner, C. M. Niemeyer, *Small* **2010**, *6*, 2162.
- [15] V. Vamvakaki, N. A. Chaniotakis, *Electroanalysis* **2008**, *20*, 1845.
- [16] M. C. Pirrung, *Angew. Chem.* **2002**, *41*, 1276.
- [17] R. Kumar, S. Weigel, R. Meyer, C. M. Niemeyer, H. Fuchs, M. Hirtz, *Chem. Commun.* **2016**, *52*, 12310.
- [18] J. H. Lee, B. S. Park, H. G. Ghang, H. Song, S. Y. Yang, *ACS Appl. Mater. Interfaces* **2018**, *10*, 13397.
- [19] B. Yang, Y. Wang, M. Vorobii, E. Sauter, M. Koenig, R. Kumar, C. Rodriguez-Emmenegger, M. Hirtz, *Adv. Mater. Interfaces* **2022**, *9*, 2102325.
- [20] K. Nawattanapaiboon, W. Kiatpathomchai, P. Santanirand, A. Vongsakulyanon, R. Amarit, A. Somboonkaew, B. Sutapun, T. Srihirin, *Biosens. Bioelectron.* **2015**, *74*, 335.
- [21] K. Gajos, P. Petrou, A. Budkowski, K. Awsiuk, A. Bernasik, K. Misiakos, J. Rysz, I. Raptis, S. Kakabakos, *Analyst* **2015**, *140*, 1127.
- [22] A. Angelin, S. Weigel, R. Garrecht, R. Meyer, J. Bauer, R. K. Kumar, M. Hirtz, C. M. Niemeyer, *Angew. Chem., Int. Ed.* **2015**, *54*, 15813.
- [23] A. Opdahl, D. Y. Petrovykh, H. Kimura-Suda, M. J. Tarlov, L. J. Whitman, *Proc. Natl. Acad. Sci. U.S.A.* **2007**, *104*, 9.
- [24] A. W. Peterson, R. J. Heaton, R. M. Georgiadis, *Nucleic Acids Res.* **2001**, *29*, 5163.
- [25] S. Watcharinyanon, D. Nilsson, E. Moons, A. Shaporenko, M. Zharnikov, B. Albinsson, J. Martensson, L. S. Johansson, *Phys. Chem. Chem. Phys.* **2008**, *10*, 5264.
- [26] S. M. Schreiner, D. F. Shudy, A. L. Hatch, A. Opdahl, *Anal. Chem.* **2010**, *82*, 2803.
- [27] M. Mrksich, *Chem. Soc. Rev.* **2000**, *29*, 267.
- [28] T. N. Ly, S. Park, S. J. Park, *Sens. Actuators, B* **2016**, *237*, 452.
- [29] G. M. Das, S. Manago, M. Mangini, A. C. De Luca, *Nanomaterials* **2021**, *11*, 2679.
- [30] L. Sun, S. Svedhem, B. Akerman, *Langmuir* **2014**, *30*, 8432.
- [31] Linette M. Demers, C. A. Mirkin, R. C. Mucic, R. A. Reynolds, R. L. Letsinger, R. Elghanian, G. Viswanadham, *Anal. Chem.* **2000**, *72*, 5535.
- [32] M. E. Minaei, M. Saadati, M. Najafi, H. Honari, *Electroanalysis* **2016**, *28*, 2582.
- [33] S. A. Jadhav, *J. Phys. Org. Chem.* **2017**, *30*, e3611.
- [34] S. M. M. Dadfar, S. Sekula-Neuner, U. Bog, V. Trouillet, M. Hirtz, *Small* **2018**, *14*, 1800131.
- [35] J. Escorihuela, M. J. Banuls, R. Puchades, A. Maquieira, *J. Mater. Chem. B* **2014**, *2*, 8510.
- [36] S. M. M. Dadfar, S. Sekula-Neuner, V. Trouillet, M. Hirtz, *Adv. Mater. Interfaces* **2018**, *5*, 1801343.
- [37] J. Escorihuela, M. J. Banuls, S. Grijalvo, R. Eritja, R. Puchades, A. Maquieira, *Bioconjug. Chem.* **2014**, *25*, 618.
- [38] J. Chen, C. Yu, Z. Shi, S. Yu, Z. Lu, W. Jiang, M. Zhang, W. He, Y. Zhou, D. Yan, *Angew. Chem.* **2015**, *54*, 3621.
- [39] S. C. Luo, H. Xie, N. Chen, H. H. Yu, *ACS Appl. Mater. Interfaces* **2009**, *1*, 1414.
- [40] C.-Y. Lee, P.-C. T. Nguyen, D. W. Grainger, L. J. Gamble, D. G. Castner, *Anal. Chem.* **2007**, *79*, 4390.
- [41] D. Y. Petrovykh, H. Kimura-Suda, L. J. Whitman, M. J. Tarlov, *J. Am. Chem. Soc.* **2003**, *125*, 5219.
- [42] C.-Y. Lee, P. Gong, G. M. Harbers, D. W. Grainger, D. G. Castner, L. J. Gamble, *Anal. Chem.* **2006**, *78*, 3316.
- [43] A. S. Yeri, L. Gao, D. Gao, *J. Phys. Chem. B* **2010**, *114*, 1064.
- [44] X. Su, Y.-J. Wu, R. Robelek, W. Knoll, *Langmuir* **2005**, *21*, 348.
- [45] S. M. D. Paul, D. Falconnet, S. P. Pasche, M. Textor, A. P. Abel, E. Kauffmann, R. Liedtke, M. Ehrat, *Anal. Chem.* **2005**, *77*, 5831.
- [46] J. Movilli, A. Rozzi, R. Ricciardi, R. Corradini, J. Huskens, *Bioconjugate Chem.* **2018**, *29*, 4110.
- [47] T. Sano, C. M. Niemeyer, C. L. Smith, C. R. Cantor, *Nucleic Acids Res.* **1994**, *22*, 5530.
- [48] R. Meyer, S. Giselbrecht, B. E. Rapp, M. Hirtz, C. M. Niemeyer, *Curr. Opin. Chem. Biol.* **2014**, *18*, 8.
- [49] A. K. Schneider, C. M. Niemeyer, *Angew. Chem.* **2018**, *57*, 16959.
- [50] W.-Y. Wang, C.-W. Hsu, K.-T. Wang, H.-A. Chen, T.-C. Wei, *Sci. Rep.* **2017**, *7*, 9656.

- [51] C. Rodriguez-Emmenegger, S. Janel, A. de los Santos Pereira, M. Bruns, F. Lafont, *Polym. Chem.* **2015**, *6*, 5740.
- [52] Y. Huang, B. B. Stogin, N. Sun, J. Wang, S. Yang, T. S. Wong, *Adv. Mater.* **2017**, *29*, 1604641.
- [53] J. Kim, P. Seidler, L. S. Wan, C. Fill, *J. Colloid Interface Sci.* **2009**, *329*, 114.
- [54] J. Ederer, P. Janoš, P. Ecorchard, J. Tolasz, V. Štengl, H. Beneš, M. Perchacz, O. Pop-Georgievski, *RSC Adv.* **2017**, *7*, 12464.
- [55] D. R. Bortz, E. G. Heras, I. Martin-Gullon, *Macromolecules* **2011**, *45*, 238.
- [56] L. Xu, F. Yao, J. Luo, C. Wan, M. Ye, P. Cui, Y. An, *RSC Adv.* **2017**, *7*, 4746.
- [57] C. R. Yuansheng Sun, V. Jyothikumar, A. Periasamy, *Cytom. Part. A* **2013**, *00A*, 00.
- [58] J. Zempleni, S. S. Wijeratne, Y. I. Hassan, *BioFactors* **2009**, *35*, 36.
- [59] G. Arrabito, S. Reisewitz, L. Dehmelt, P. I. Bastiaens, B. Pignataro, H. Schroeder, C. M. Niemeyer, *Small* **2013**, *9*, 4243.
- [60] M. Hirtz, A. M. Greiner, T. Landmann, M. Bastmeyer, H. Fuchs, *Adv. Mater. Interfaces* **2014**, *1*, 1300129.